Landslide Mechanism of a Slope in Nanhuan Road, Funxin, Northeast China

Huiming Liu*, Changming Wang, Suoyu Zhang, Bing Wang

*College of Construction Engineering, Jilin University, Changchun 130026, China

(hmliu15@mails.jlu.edu.cn)

Abstract

Targeted at a slope in Nanhuan Road, Fuxin, Northeast China, this paper explores the cause and failure mechanism of landslide through site survey, surface displacement monitoring, inclinometer measurement, and limit equilibrium analysis. It is concluded that the landslide is mainly attributable to the load increase on slope crest induced by subgrade backfill and the rise in groundwater table resulted from rainfall infiltration. The results of the monitoring and limit equilibrium analysis show that 2 slip surfaces were placed at reasonable positions in the slope. Through the analysis of monitoring results, the mechanism of the landslide is summarized as grading creeping-sliding mechanism. Finally, the sliding mass was portioned to lay the basis for further slope management.

Key words

Landslide, Slope stability, Formation mechanism, Backfill, Rainfall infiltration.

1. Introduction

Landslide is a common geological hazard that incurs serious personal and property losses in mountainous regions. The mechanical properties behind the hazard depend on various inter-correlated factors. The previous research has shown that landslide might be initiated or reactivated under the following three conditions in the highway and railway engineering. First, the original landform of the slope along the route has been changed by toe cutting or surface loading; Second, the pore water pressure has increased in the low permeable slope after heavy seasonal rainfall, leading to reduced rock strength; Third, the slope has been hit by earthquake or blasting.

Some of the most popular tools of slope stability analysis include the limit equilibrium method and the 2D~3D limit analysis methods based on the upper bound theorem. With the development of computer technology, the finite-element method has been applied to slope stability analysis, making it possible to set more stringent conditional assumptions and analyse the stress and strain of the slope. These methods should be combined with the actual engineering conditions to perform accurate analysis of slope stability and landslide causes.

In this research, the object is a slope located on the south of the K13~14 section of Nanhuan Road in Fuxin, a city in Northeast China. The multi-layered slope is formed with the slags produced by surrounding mines after many years. Nanhuan Road passes through the top of the slope, while another road (Yimin Road) and a village (Nanwa) are located at the bottom of the slope. Since October 2012, the subgrade of Nanhuan Road has been undergoing continued settlement deformation, resulting in numerous cracks and obvious deformation at all steps of the slope. What is worse, a large area of surface deformation has appeared at the slope bottom, posing a major threat to the Yimin Road and residential buildings in Nanwa Village. In order to disclose the formation and sliding mechanism of the landslide, this paper carries out site survey, surface displacement monitoring, inclinometer measurement, and physical and mechanical tests. Based on the results, the author established a model for the slope, analysed the slope stability by limit equilibrium method, and partitioned the slope to reveal the sliding mechanism.

2. Description of Landslide

The study area and the location of the slope are shown in Fig.1. The clear steps on the slope reflect the stages of backfilling by the surrounding mines. A three steps slope was formed at the end of backfilling in 2004 (Fig.1.a). The slope was originally stable and free from deformation. However, the stability was undermined by the construction of Nanhuan Road from March to September 2012. The road crossed the top of the original slope at Step 3 from northeast to southwest. A largescale backfilling was carried out to meet the road design requirements. The backfill formed a new step (Step 4) atop the original slope (Fig.1.b). After the construction, the slope can be divided into four steps, each of which consists of a 25~35° slope and a relatively flat platform. From bottom to top, Step 1, Step 2 and Step 3 are all 20m tall, and Step 4 is about 15m in height (Fig.1.b).

In October 2012, cracks were observed in the K13+500 section of Nanhuan Road, marking the beginning of slope deformation, but no sliding feature was found. In response to the deformation, the highway maintenance department treated subgrade settlement by excavation and

backfill, and excavated the subgrade slope to reduce the load. Unfortunately, cracks reappeared at the original position only 2 months after the renovation. The same maintenance activities were performed again, but to no avail. Neither did the injection grouting in the third maintenance achieve any practical effect.
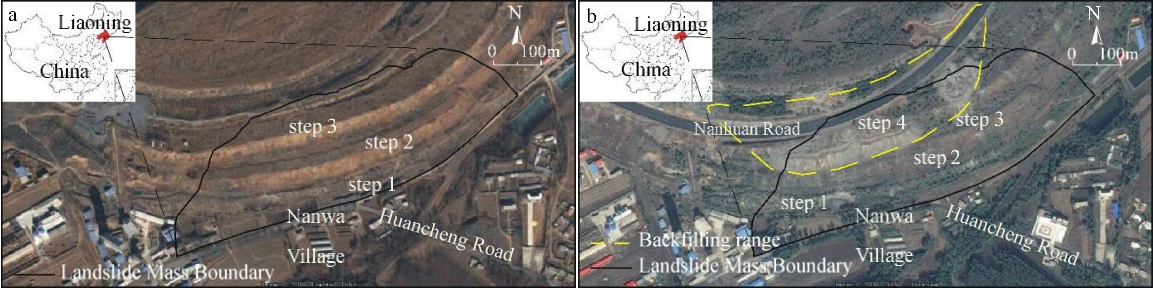

Fig.1. Location of the Study Area (a. Before backfilling b. After backfilling)

In August 2013, the first sign of ground heave was recorded at the intersection of Yimin Road and Huancheng Road at the bottom of the slope. Besides, cracks and sliding features were discovered on the slope of Step 1. Two months later, the area of cracked pavement on Nanhuan Road further expanded, leaving three obvious cracks on the pavement. The cracks were up to 340m in length and 1~30cm in width. The height difference between the two sides of crack was 20cm at the most. According to the observation data, the maximum road settlement was 15.1cm, and the maximum crack width was 12cm from August to September in 2013.
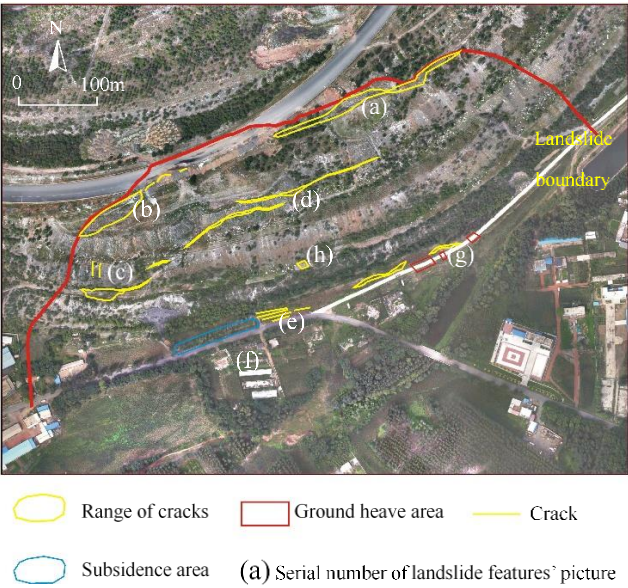

Fig.2. Location of Landslide Features in the Site Survey in September 2015

As the road continued to settle with the deformation of the slide mass, a number of backfills were performed on the subsidence section by the road maintenance department. The site survey in September 2015 shows that the total pavement settlement had surpassed 5m, clear boundaries had formed around the slide mass, and a number of cracks had formed on the surface of the slide mass (Fig.2.). At the bottom of the slope, the deformation had induced uneven settlement of Yimin Road, ground heave in the surrounding residential areas, and cracking on the walls of residential buildings (Fig.3.).
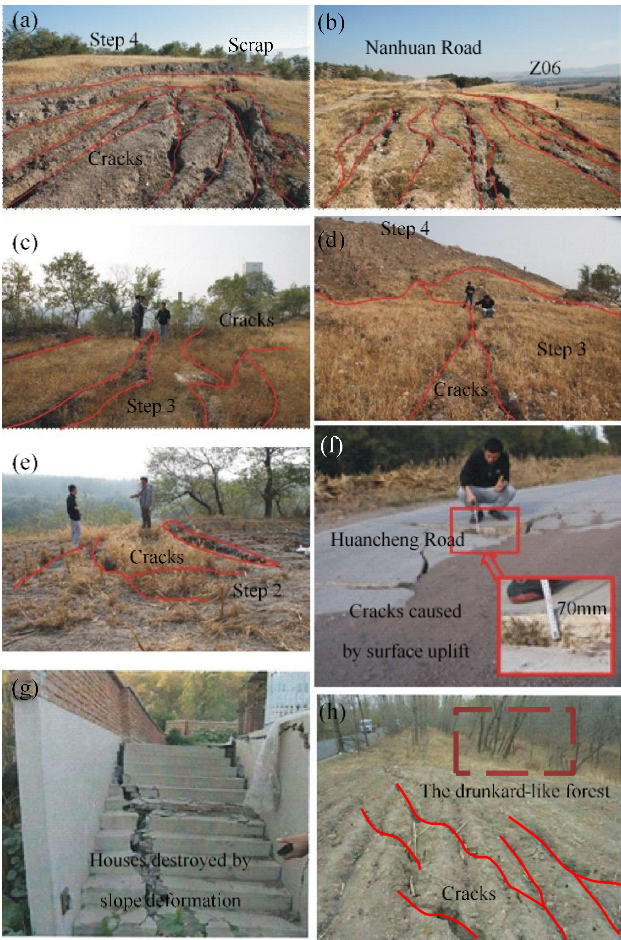

Fig.3. Most Evident Damages of the Nanhuan Road Landslide

3. Methodology

3.1 Site Survey

A site survey was conducted to ascertain the distribution of the sliding features on the slope surface and evaluate the slope stability and development trend of landslide. Fig.4. shows the

location of monitoring points, boreholes and section lines, and illustrates the distribution of slope deformation features. Fig.5. details a typical longitudinal section I-I' extracted from Fig.4. and displays the stratigraphic information obtained from the boreholes. As shown in the figure, the slope is formed with the slags produced by surrounding mines. The upper part of the gangues is a 4.2~64.4m thick layer of sandstone, mudstone and sub-clay, while the lower part of the gangue is a 1.2~12.0m thick layer of silty clay. The lower part used to be the surface soil layer before the accumulation of slags. The bedrock is composed of weathered sandstone. The ground water table was measured based on the monitoring results of drilling. The relevant engineering geological parameters of the slope were tested according to the relevant requirements of the Code for Investigation of Geotechnical Engineering (GB50021-2009). The test results are summarized in Table 1.
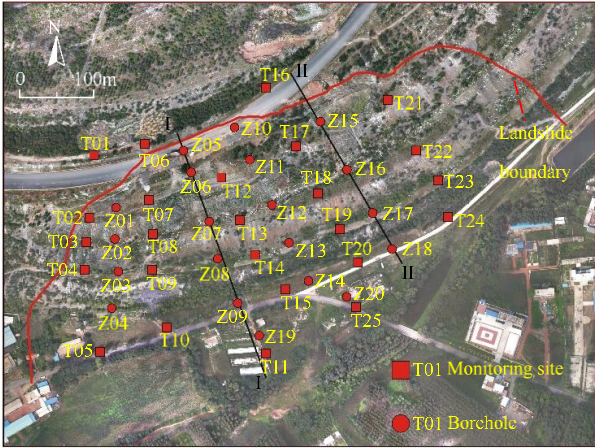

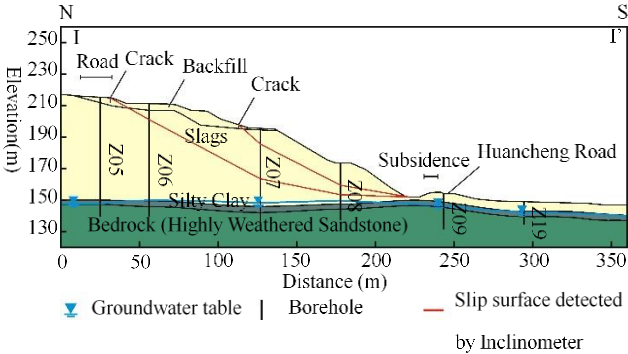Fig.4. Location of Monitoring Points, Boreholes and Section Lines

Fig.5. Cross-section I-I′ of the Slope

Table 1. Physical Properties of the Slope

Parameter	Condition	Unit weight γ (kN/m^3)	Cohesion c (kpa)	Friction angle φ (°)
Slag	Unsaturated	18.5	12.0	26.0
	Saturated	19.0	2.0	20.0
Silt clay	Unsaturated	19.9	64.0	19.7
	Saturated	20.3	0	15.0
Bedrock	Unsaturated	20.2	64.0	20.0

3.2 Slide Meichuangass Monitoring

3.2.1 Surface Displacement Monitoring

After the site survey of the landslide, 24 surface displacement monitoring points (T01-T24) were set up on the surface of the slide mass and in the surrounding area, aiming to capture the sliding trend in different areas (Fig.4).

The monitoring is divided into two phases. Phase 1 lasts from September 11 to November 12, 2015, and Phase 2 from November 25, 2015 to February 28, 2016. To directly reflect the deformation in different ranges on the same platform, a uniform date was set as the start time of monitoring. The sliding trend was studied by analyzing the variation in the horizontal and vertical displacements of the monitoring points in the same time period.

On the top platform (Step 4) of the slope (Fig.6), all the monitoring points underwent obvious displacement in the horizontal direction. The horizontal displacement increased with the monitoring time. During the monitoring process, the most pronounced displacement increments were measured at T02, T07 and T12, all of which fell in the range of 219mm~227mm at the end of Phase 2. In the vertical direction, all the monitoring points on this platform exhibited apparent settlement. The vertical settlement also increased with the monitoring time. The most prominent vertical settlements were measured at T12 and T17 in Phase 1. The settlement values of T07, T02 and T21 were very close to each other. In Phase 2, the settlement of T21 gradually slowed down. At the end of Phase 2, T12 and T17 had the greatest settlements (331mm vs. 271mm), followed by T02 and T07, both of which shared similar degree of settlement (240mm); the minimum settlement was observed at T21 (177mm).

To sum up, T12 underwent the significant displacement in both directions, T02 and T07 were mainly displaced in the horizontal direction, T17 was mainly displaced in the vertical direction, and T21 had unobvious displacement in either direction.
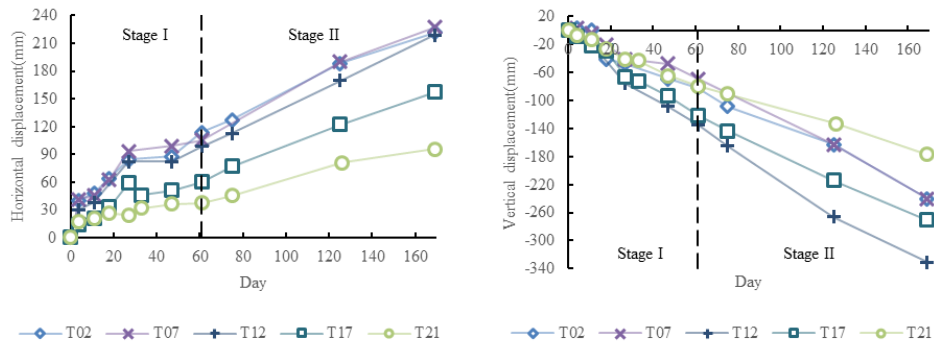
Fig.6. Displacement of Step 4

The monitoring points in Step 3 of the slope exhibited different displacement features (Fig.7). The monitoring points underwent horizontal displacement along the direction of the slope, and the displacement value increased steadily with the growth of the monitoring time. At the end of Phase 2, the monitoring points were ranked as T13> T18> T08> T22> T03 in descending order of displacement. In the vertical direction, each monitoring point in this platform underwent significant deformation. The settlement also increased steadily with the growth of the monitoring time. At the end of Phase 2, T03 and T08 had the most obvious settlements (142mm vs. 116mm), while the settlements of T13, T18 and T22 fell in the interval of 37mm~42mm.

In short, T08 underwent the significant displacement in both directions, T13, T18 and T22 were mainly displaced in the horizontal direction, and T03 was mainly displaced in the vertical direction.
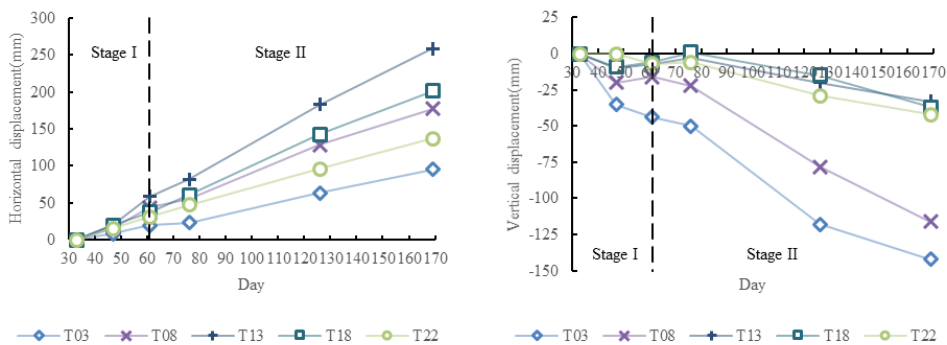

Fig.7. Displacement of Step 3

As shown in Fig.8, all of the monitoring points on Step 2 exhibited obvious displacement in the horizontal direction, which increased with the monitoring time. At the end of Phase 1, the monitoring points were ranked as T09> T14> T19> T23> T04 in descending order of displacement. In the vertical direction, the monitoring points differed markedly in the deformation trend. As the

490

monitoring time increased, the vertical settlement of the monitoring points showed great uncertainty. For instance, T04 experienced varied degrees of settlement and uplift during the monitoring: the final trend was settlement (28mm) at the end of Phase 2. For the monitoring point T09, the vertical deformation was an uplift (max: 10mm) at the beginning of Phase 1, the uplift and settlement appeared alternatively during Phase 1, and trend was settlement (9mm) at the end of Phase 1; the uplift and settlement appeared alternatively again during Phase 2, and the final trend was uplift (3mm) at the end of Phase 2. The monitoring point T14 experienced uplift (max: 5mm) and settlement (max: 7mm) alternatively during Phase 1. During the monitoring period, the displacement trend of T19 was mainly manifested as settlement, and the final settlement was 41mm at the end of Phase 2. For the monitoring point T23, settlement was the main displacement trend in Phase 1 and the final settlement reached 20mm at the end of Phase 2; of course, there was a slight uplift trend at the beginning of Phase 2.
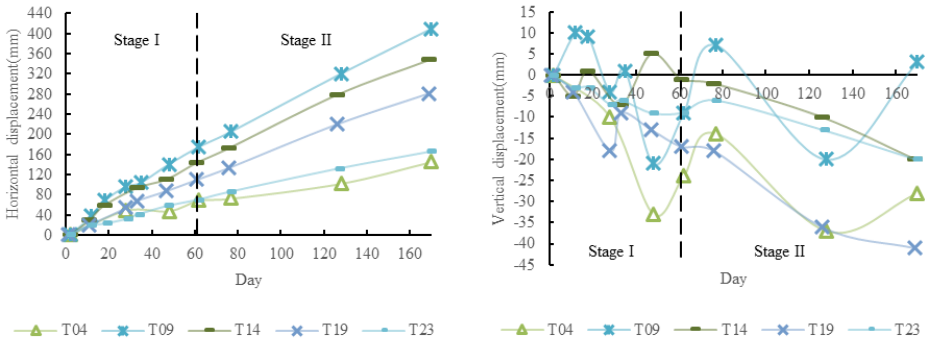

Fig.8. Displacement of Step 2

As shown in Fig.9, all of the monitoring points on Step 1 exhibited obvious displacement in the horizontal direction. At the end of Phase 2, the monitoring points were ranked as T10> T20> T19> T15 in descending order of displacement. There was also significant deformation in the vertical direction at these monitoring points, that is, a steady increase in the uplift with the growth of the monitoring time. At the end of Phase 2, the maximum uplift occurred at T15 (192mm). T10 and T20 had similar uplifts, which varied between 67mm and 92mm.
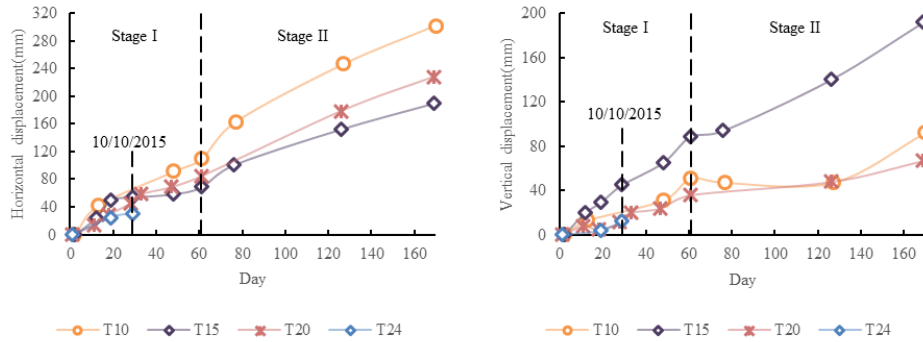
491

Fig.9. Displacement of Step 1

3.2.2 Analysis of Surface Monitoring Results

The deformation pattern of the slope was analyzed from two aspects: the per unit time displacement of the monitoring points on the same step, and the displacement of monitoring points in a straight along the sliding direction of the landslide.

For the monitoring points on Step 4, the horizontal displacement was consistent with the sliding direction of landslide, and the vertical deformation was displayed as settlement. The settlement of the monitoring points (T02, T07, T12) in backfill area was greater than the one (T21) in the original area.

Step 3 was formed by the accumulation of slags. The shape of the slope had a great impact on the horizontal deformation. Under the impact, the monitoring points on the edge (T03, T22) underwent the smallest horizontal displacements, while the monitoring point in the protruding position (T13) had a much greater horizontal displacement. At the beginning of the monitoring, T03 boasted the greatest vertical displacement under the action of the backfill subgrade on Step 4. The deformation of T03, in turn, affected the surrounding area, such as inducing major growth of the vertical displacement of T08. With less impact of backfill and surrounding settlement, there was no significant increase in the vertical displacements of T13, T18 and T22.

Step 2 had a similar horizontal displacement to Step 3. The monitoring points on the edge (T03, T22) underwent the smallest horizontal displacements, while the monitoring point in the protruding position (T09, T14) had the largest horizontal displacements. In the vertical direction, the monitoring points on Step 3 experienced irregular uplift and settlement during the monitoring period. Hence, it is assumed that Step is located on and affected by multiple sliding surfaces.

Situated at the bottom of the slope, Step 1 was severely squeezed by the upper sliding mass. Under the squeezing effect, the monitoring points on the step exhibited a large displacement. The effect of the sliding mass also led to the pronounced uplift at the bottom.

492

All in all, the backfill area had much greater horizontal and vertical displacement than the original slope area. In the same step, the horizontal deformation was mainly influenced by the shape of slope, while the vertical deformation hinged on the upper load.

3.2.3 Measurement of Cumulative Displacement

To determine the sliding direction of the whole slope, the author took the first measured coordinates of the monitoring points and boreholes as the base points, and calculated the displacement and directions of each monitoring point by adding up the measured data from two different measurement phases (Fig.10). The monitoring points with an error no greater than 30mm in the horizontal direction and 20mm in the vertical direction were called relatively stable points. According to cumulative displacement in the two phases, T01, T05, T06, T11, T16, T24, T25 (monitoring points) and Z15, Z20 (boreholes) were named as relatively stable points.

In Phase 1 (Fig.10.a, c), T09 was the most horizontally displaced monitoring point (175mm), T12 was the most vertically displaced monitoring point (135mm), Z03 was the most horizontally displaced borehole (176mm), and Z06 was the most vertically displaced borehole (137mm). The measured results of Phase 2 are independent of those of Phase 1. In Phase 2, the displacement of each monitoring point increased in varied degrees (Fig.10.b, d). The results are as follows: T09 was the most horizontally displaced monitoring point (235mm), T12 was the most vertically displaced monitoring point (196mm), Z08 was the most horizontally displaced borehole (221mm), and Z06 was the most vertically displaced borehole (195mm).

Sorting out the monitoring results, it was concluded that the horizontal displacements of the monitoring points fell in 150°~180°. According to the direction of displacement, the landslide was determined as south-trending, and the middle part of the sliding mass was the hotbed of landslide.
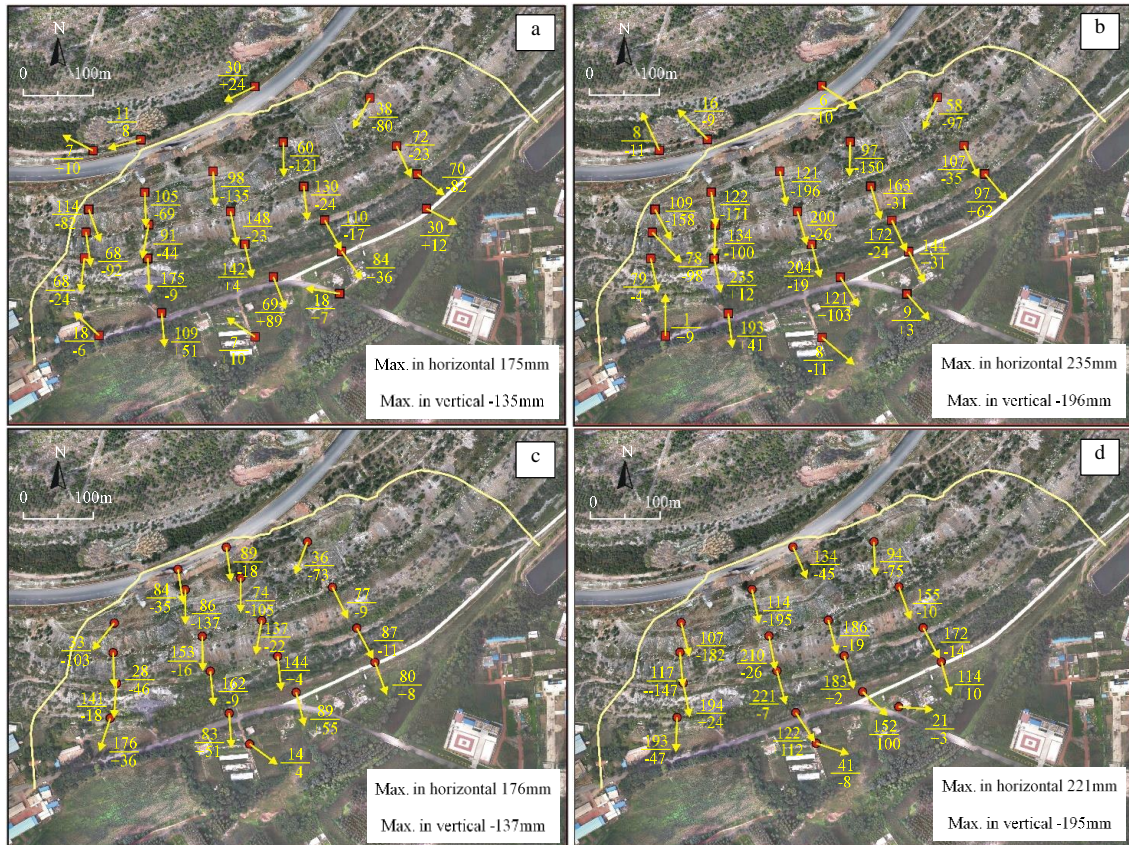
3.2.4 Inclinometer Measurement

Fig.10. Displacement of monitoring points and boreholes (a. Displacement of monitoring points during Phase 1. b. Displacement of monitoring points during Phase 2. c. Displacement of boreholes during Phase 1. d. Displacement of boreholes during Phase 2. Note: The horizontal and vertical displacements were measured at the slope from September 2015 to February 2016. As for the fraction $\frac{A}{\pm B}$ in the figure, A is the horizontal displacement, B is the vertical displacement, + is the uplift, and – is the settlement.)
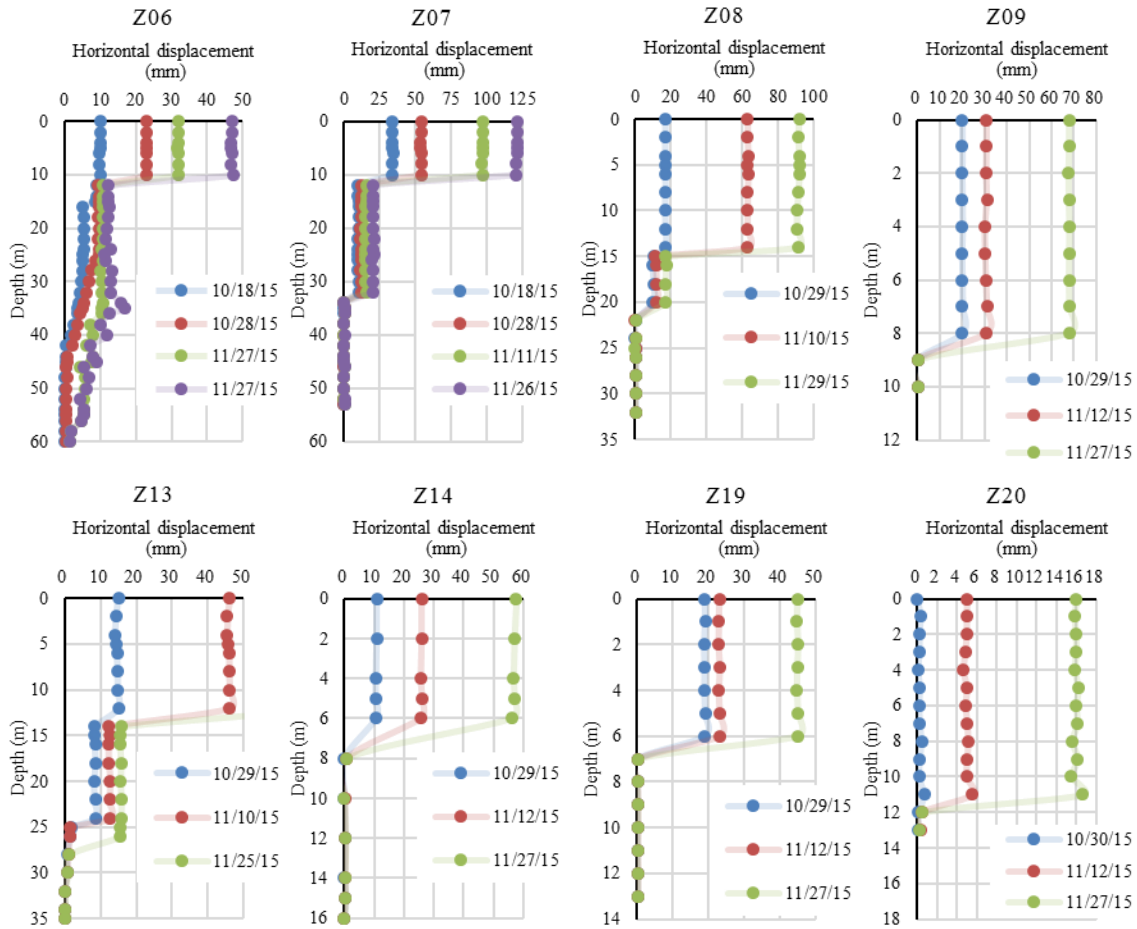
Fig.11. Horizontal Displacement Profiles of the Slope

After the site survey, the inclinometer measurement of the slope was conducted from October 2015 to November 2015. With the boreholes as the monitoring holes, an inclinometer was adopted to measure the horizontal displacement of each borehole at different depths. The selected boreholes include Z06 (depth: 60m), Z07 (depth: 53m), Z08 (depth: 32m), Z09 (depth: 10m), Z13 (depth: 35m), Z14 (depth: 16m), Z19 (depth: 13m) and Z20(depth:13m). During the measurement period, Z06 underwent 1 relative displacement at the depth of 15m; Z07 underwent 2 relative displacements at the depths of 10m and 32m; Z08 underwent 2 relative displacements at the depths of 14m and 20m; Z09 underwent 1 relative displacement at the depth of 8m; Z19 underwent 1 relative displacement at the depth of 6m. The measurement results reveal that the slope was still in the process of sliding. The locations of two sliding surfaces can be initially identified based on the site survey and inclinometer measurement.

4. Slope Stability Analysis Based on Limit Equilibrium Method

495

In light of the surface displacement monitoring data, the section with the most significant displacement along the sliding direction, i.e. section I-I', was selected as the typical section for slope stability analysis. The Morgenstern-Price (M-P) method was introduced to compute the slope stability, as it was assumed that the slip surface is not a circular sliding surface. Table 1 lists the calculation parameters obtained from the pre-survey test. Three types of conditions were configured for the slope stability analysis in different phases. In condition 1, the subgrade backfill was not performed and the slope was in the natural state. In condition 2, the subgrade backfill had been finished but the slope was not affected by rainfall infiltration. In condition 3, the slope had been affected by rainfall infiltration.
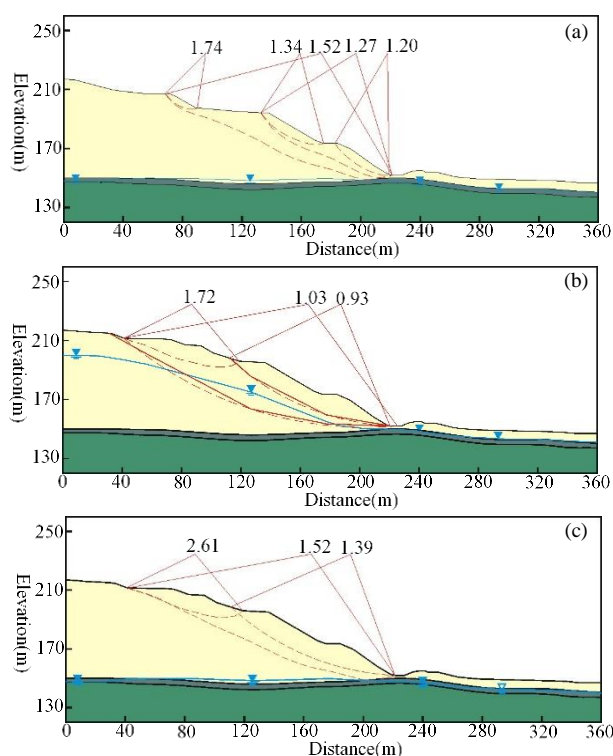

Fig.12. Slope Stability Analyses in Different Conditions (a. Before backfill b. After backfill c. The effect of rainfall infiltration)

In condition 1, the whole slope consisted of 3 steps. The safety factor was 1.52 for the whole slope, 1.27 for Steps 1 & 2, and 1.20, 1.34 and 1.74 for each of the three steps in ascending order. The safety factors demonstrate that the slope was in the stable state in condition 1 (Fig.12. (a)).

In condition 2, two tensile fractures were selected as the trailing edge of the slope according to the landslide features acquired in the site survey. Then, three sliding surfaces were identified

496

after checking the stability of each step. The safety factor was 1.52 for the whole slope, 2.61 for Steps 3 & 4, and 1.39 for Steps 1, 2 & 3. The safety factors indicate that the slope was still in the stable state in condition 2 (Fig.12. (b)).

In condition 3, the groundwater table rose in the slope under rainfall infiltration. The slope stability was checked in the same way as in condition 2. The safety factor was 1.03 for the whole slope, 1.72 for Steps 3 & 4, and 0.93 for Steps 1, 2 & 3. This means the slope was in the failure state (Fig.12. (c)).

The calculated results are in good agreement with the data measured by the inclinometer. The two slip surfaces are basically reasonable, because the slags were not accumulated evenly year after year.

5. Segmentation of the Slide Mass

Based on the results of site survey, surface displacement monitoring, inclinometer measurement and limit equilibrium, the slide mass was segmented according to the sliding rate and the deformation features (Fig.13.).

Region 1: According to the results of surface displacement monitoring, this region has the greatest settlement in the sliding area, and a relatively insignificant horizontal displacement. During the construction of Nanhuan Road, the subgrade backfill added to the load on the slope crest, resulting in the settlement of the whole slope. In return, the settlement deformation led to the tensile fracture of the road and shear cracking on the edge of the primary sliding surface.

Region 2: This region is located between the two tensile fractures resulted from the sliding surface. There are two effects of subgrade backfill during the construction of road. On the one hand, the original slope experienced a typical settlement due to subgrade settlement and backfill soil weight; on the other hand, a more pronounced displacement occurred in the main sliding direction under the deformation squeezing of the subgrade backfill. Under the joint effect of horizontal and vertical deformations, Nanhuan Road was displaced by over 5m in this region.

Region 3: Situated on the outside of the subgrade backfill area, this region is still affected by the deformation of the backfill area. The upper part of the region has several tensile fractures, which become narrower as the distance from the backfill area increases. Since the backfill was not conducted in this region, the vertical displacement here in much smaller than that in Regions 1 and 2.

Region 4: This region is located within the secondary sliding surface. The whole slide mass slid down along the slope direction. With the extrusion of deformations in Regions 1 and 2,

however, the stress in the slide mass was distributed abnormally, creating irregular settlement and uplift.

Region 5: Located in the middle of the slide mass, this region shares a similar sliding situation with Region 3. Under the joint action of settlement and sliding in Region 2, the tensile fractures created by the secondary sliding surface tended to expand during the monitoring process.

Region 6: This region partially falls in the secondary sliding surface and partially on the sliding boundary. Hence, it was influenced by the deformation of Region 3 and a part of secondary sliding surface. Of course, the deformation effect from Region 3 was unobvious for the latter stayed beyond the backfill area. Besides, the regional displacement decreased with the increase in the distance from the sliding surface.

Region 7. This region is located in the south of the slope foot. Here, the surface deformation was manifested as uplift. The surrounding buildings were deformed and destroyed, and the pavement of Huancheng Road underwent wavy uplift and tilt.
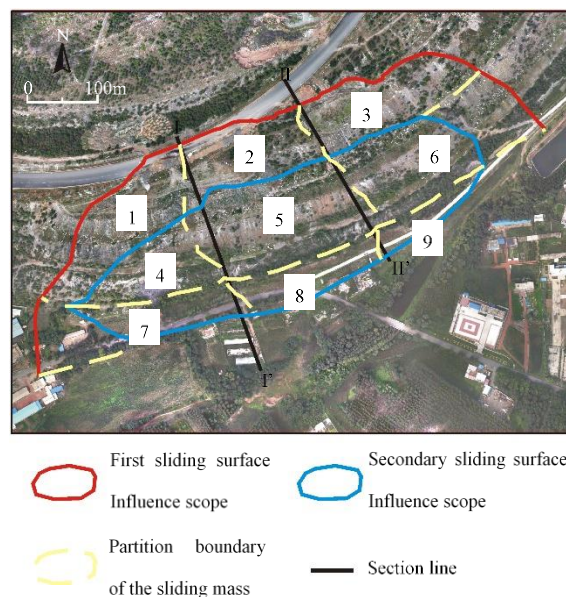

Fig.13. Segmentation of the Slide Mass Based on the Investigation Results

Region 8: The region is located in the middle of the slope foot. The surface deformation was also manifested as uplift. The walls of the residential buildings were damaged and covered with tensile fissures. The road pavement was hit by severe settlement (max: 5m).

498

Region 9: The region is located on the north of the slope foot. The surface deformation was exhibited as slight uplift with small regional elevation. The road pavement cracked and slightly uplifted.

6. Mechanism Analysis of the Landslide

According to the results of site survey, the cracks on the Nanhuan Road atop the slope were mainly caused by the deformation of the subgrade backfill. The slope stability was weakened by the load increase on slope crest induced by injection grouting and the rise in groundwater table resulted from rainfall infiltration. Through the inclinometer measurement and limit equilibrium analysis, it is concluded that the slope has two sliding surfaces, and that the landslide is a multiple unstable landslide. The conclusions are evidenced by the cracks, scarps, ground fissures and surface uplifts observed in the site survey and the data acquired through the monitoring.

The landslide mechanism is known as "grading creeping-sliding". There are two main inducements of the landslide: subgrade backfill and rainfall infiltration. The slope contains two sliding surfaces similar in deformation evolution. One cuts through the whole slide mass, and the other slides through Steps 1, 2 and 3. During the construction of Nanhuan Road, the subgrade backfill intensified the load on the slope crest; furthermore, the settlement deformation of the backfill resulted in cracks on the road pavement, creating a favorable condition for rainfall infiltration. When the rainwater infiltrated the slope, the groundwater table climbed up, weakened the slope strength and enhanced the bulk density. Then, the slope started to creep under the deadweight. As the deformation accumulated, tensile cracks and scarps emerged at the top of the slope, and surface uplift and ground fissures appeared at the bottom. Meanwhile, one or more failure surfaces came to being. Once the driving forces exceeded the resisting forces, the slide mass began sliding. At this time, the safety factor of the whole slope was 1.03, indicating that the slope was in the state of limit equilibrium. In order to maintain the normal operation of the road, several backfill operations were carried out to curb the deformation in the backfill area. These operations further increased the load on the slope crest, accelerated the deformation of the slope, and jeopardized slope stability. In this case, the safety factor was 0.93 for Steps 1, 2 & 3, revealing that the slope had entered the state of instability. Large tensile fractures were seen on Step 3, and obvious deformation was observed at the foot of the slope. Under the combined action of the slope crest load and rainfall infiltration, the slope slid in the monitoring period, forming two sliding surfaces.

Conclusions

Targeted at a slope in Nanhuan Road, Fuxin, Northeast China, this paper explores the cause and failure mechanism of landslide through site survey, surface displacement monitoring, inclinometer measurement, and limit equilibrium analysis. During the research, the slope features were described and the inducements to landslide mechanism were discussed one after the other. In the end, several conclusions were drawn as follows:

(1) The landslide of the study area is mainly caused by rainfall infiltration and subgrade backfill. The backfill soil increased the load atop the slope, while the rainfall infiltration pushed up the groundwater table. The rising groundwater level, in turn, added to the weight of the slope mass and weakened the strength of the soil.

(2) Based on the site survey and surface displacement monitoring, the slope was divided into 9 regions in light of the slide mass deformation. Among them, Regions 1, 2, 4 and 5 had the most obvious deformation. These regions should be prioritized in slope management in future research.

(3) Two typical sliding surfaces were determined in the slope through site survey, inclinometer measurement and limit equilibrium analysis. The results of surface monitoring indicate that the mechanism of the landslide is "grading creeping-sliding". It is necessary to tackle the extrusion effect in the creep stage of the landslide.

References

1. A. Lulseged, Y. Hiromitsu, M. Hideaki, Landslides in Sado Island of Japan: Part I. Case studies, monitoring techniques and environmental considerations, 2005, Engineering Geology, vol. 81, no. 4, pp. 419-431.

2. E. Steiakakis, K. Kavouridis, D. Monopolis, Large scale failure of the external waste dump at the "South Field" lignite mine, Northern Greece, 2009, Engineering Geology, vol. 104, no. 3-4, pp. 269-279.

3. L. Xu, Q. Wang, J. Chen, Formation mechanism of Ermi landslide, 2012, Journal of Jilin university (Earth science edition), vol. 42, no. 4, pp. 1104-1111.

4. K.E. Obermiller, M.M. Darrow, S.L. Huang, Site investigation and slope stability analysis of the Chitina Dump Slide (CDS), Alaska, 2013, Environmental & Engineering Geoscience, vol. 19, no. 1, pp.27-40.

5. G. Prountzopoulos, P. Fortsakis, K. Seferoglou, Assessment of failure mechanism and rehabilitation of a landslide within marly formations in NW Greece: From the site investigation

to the geotechnical design, 2014, Geotechnical and Geological Engineering, vol. 32, no. 6, pp. 1485-1502.

6. D. Xue, T. Li, Y. Wei, M. Gao, Mechanism of reactivated Badu landslide in the Badu Mountain area, Southwest China, 2014, Environmental Earth Sciences, vol. 73, no. 8, pp. 4305-4312.

7. W. Jian, Q. Xu, H. Yang, Mechanism and failure process of Qianjiangping landslide in the Three Gorges Reservoir, China, 2014, Environmental Earth Sciences, vol. 72, no. 8, pp. 2999-3013.

8. K. Anbarasu, A. Sengupta, S. Gupta, Mechanism of activation of the Lanta Khola landslide in Sikkim Himalayas, 2010, Landslides, vol. 7, no. 2, pp. 135-147.

9. Q. Xu, L. Zhang, The mechanism of a railway landslide caused by rainfall, 2010, Landslide, vol. 7, no. 2, pp. 149-156.

10. G. Wang, Kinematics of the Cerca del Cielo, Puerto Rico landslide derived from GPS observations, 2012, Landslide, vol. 9, no. 1, pp. 117-130.

11. S.S. Chandrasekaran, R.S. Owaise, S. Ashwin, Investigation on infrastructural damages by rainfall-induced landslides during November 2009 in Nilgiris, India, 2013, Natural Hazards, vol. 65, no. 3, pp. 1535-1557.

12. Y. Yin, B. Li, W. Wang, Dynamic analysis of the stabilized Wangjiayan landslide in the Wenchuan Ms 8.0 earthquake and aftershocks, 2015, Landslides, vol. 12, no. 3, pp. 537-547.

13. J Deng, H. Kameya, Y. Miyashita, Study on dip slope failure at Higashi Takezawa induced by 2004 Niigata-ken Chuetsu earthquake, 2011, Soils and foundations, vol. 51, no. 5, pp. 929-943.

14. Q.J. Xu, L.M. Zhang, W.C. Wang, Biotechnical means of soil stabilization using willow cuttings, 2009, Journal of Soil and Water Conservation, vol. 64, no. 2, pp. 105-119.

15. N.R. Morgenstern, V.E. Price, The analysis of the stability of general slip surfaces, 1965, Geotechnique, vol. 15, no. 1, pp. 79.

16. G. Liu, X. Zhuang, Z. Cui, Three-dimensional slope stability analysis using independent cover based numerical manifold and vector method, 2017, Engineering Geology, vol. 225, no. 3-4, pp. 83-95.